

(51) Examples of Electronic Structures: *Silicon* is a prototypical semiconductor with bandgap 1.12 eV and tetrahedrally coordinated Si atoms forming the diamond-type structure, space group $Fd\bar{3}m$ and two Si atoms in the primitive unit cell. The band structure shows four bands below the Fermi level. The DOS curve more clearly reveals a small bandgap between the occupied *valence band* and unoccupied *conduction band*. However, this calculated bandgap is smaller than the experimental value, a result that is typical for DFT calculations. According to the band structure, the bandgap is *indirect* because the wavevectors at the top of the valence band (Γ) and bottom of the conduction band (a Δ -point near X along the Γ -X line) are different. The COHP curve indicates optimal Si–Si bonding. A common bonding picture for silicon is to use sp^3 hybrid orbitals involved in four two-center, two-electron bonds at each Si atom. This picture is valid because there is an energy gap between occupied and unoccupied orbitals. The electronic structure hints at this hybridization as indicated by significant 3s contributions in the conduction band. According to the 3s partial DOS curve, the 3s character is largest near the bottom of the valence band and steadily decreases toward the Fermi level. There is additional 3s character in conduction band states just above the Fermi level. The variation in 3s contribution to the occupied valence band states is more clearly revealed in the band structure: the symmetry associated with the zone center, wavevector Γ , is the full point symmetry of the structure, i.e., $m\bar{3}m$. As a result, the 3p AOs form a triply degenerate crystal orbital at the Γ -point and is the top of the occupied valence band. Moving to wavevectors away from Γ reveals the degeneracy.

(52) *Aluminum phosphide* is another tetrahedral semiconductor with a bandgap of 2.45 eV and a structure that is an alternating decoration of the diamond network. The space group remains cubic $F\bar{4}3m$ and there is one AIP formula unit per primitive unit cell. The outcome on the electronic structure creates a *direct* energy gap at the Fermi level. Orbitals below the Fermi level are Al–P bonding; those above are Al–P antibonding. The occupied states have more P character than Al character because P is more electronegative than Al; the inverse is seen for the empty conduction band. Lastly, the degeneracies of the 3s and 3p AOs in the band structure at Γ remain, but other degeneracies, such as near X, are broken in AIP as compared to Si because the symmetry of AIP is symmorphic whereas the symmetry of Si is nonsymmorphic due to the presence of *d*-glide reflections.

(53) *Aluminum diboride* is a hexagonal, metallic main group compound that consists of graphenetype B nets alternating with close packed Al planes along the *c*-axis. The band structure contains numerous bands with no clear bandgaps, in agreement with the metallic properties. For the hexagonal Brillouin zone, the bands are plotted in the $k_3 = 0$ plane along Γ -K-M- Γ , then along the c^* direction Γ -A, and finally in the $k_3 = \frac{1}{2}$ plane along A-L-H-A. The DOS curve shows a distinct broad minimum between two peaks; this feature is called a *pseudogap*. The Fermi level for AlB_2 falls in this pseudogap. Also, there is strong mixing of both Al and B valence orbitals throughout the entire energy range, an outcome that suggests the electronegativity difference between Al and B is not that large. Lastly, a bonding analysis can be accomplished by examining the COHP curves: (i) the B–B as well as the B–B π -COHP curves cross from bonding to antibonding states just below the Fermi level; and (ii) the Al–B interactions are weakly bonding (essentially nonbonding) close to the Fermi level. As a result of this bonding analysis, B is considered formally isovalent with C, which is corroborated by its local structure in AlB_2 .

(54) A quantitative bonding analysis involves evaluating the percent of the total *integrated* COHP (ICOHP) values contributed by each type of interaction. These percentages are obtained by evaluating the ICOHP values for each pairwise interaction: in MB_2 , these are 3 B–B nearest

neighbor bonds within the hexagonal nets, 12 M–B contacts, and 8 M–M interactions, 2 of which are along the *c*-direction and 6 in the *ab*-plane. Then, the ICOHP value for each bond is multiplied by the number of contacts per formula unit and all these values are summed. Finally, each contribution is evaluated as a percentage. This approach allows some level of comparison between different compounds. NOTE: Because the basis set is not spatially orthogonal, all ICOHP values will depend on the specific zero-point energy for the DFT calculation (it is not the Fermi level!). For this reason, it is unwise to compare ICOHP values between different compounds. However, the percentage contributions are a satisfactory compromise when comparing a sequence of chemical structures.

(55) Electronegativity Effects: The main contributor to the position of energy bands in a DOS curve is the AO energy associated with the orbitals from which the band mostly originates. Valence AO energies tend to decrease across a period, and they tend to increase down a group. An AO energy is a measure of the *valence state ionization energy*, which is the energy required to remove an electron from the AO in the ground state configuration. These energies can be determined from experimental atomic spectra of the neutral atoms and positive ions, or they can be calculated from Hartree-Fock calculations on the atoms.

As an example of the effects of AO energies and, therefore, electronegativities, let's examine the DOS curves for the isostructural series CaO, ScN, and TiC, all of which adopt the NaCl-type structure. The trend in anion electronegativity increases from C to N to O, whereas the effective nuclear charges increase among the cations Ca to Sc to Ti. Both the anion and cation are octahedrally coordinated. Along the series CaO-ScN-TiC, the following characteristics of the DOS curves emerge:

- The position of the anion $2p$ -band in the DOS increases as the electronegativity of the anion decreases. CaO has a clear energy gap between occupied and unoccupied levels. ScN also shows an energy gap, but it is much smaller, appropriate for a semiconductor. TiC has a pseudogap, indicative of semimetallic character.
- The dispersion or bandwidth of the anion $2p$ -bands increases. This effect can be attributed to stronger cation–anion orbital interactions from CaO to ScN to TiC. The strength of orbital interactions between different atoms can be gauged by the ratio $H_{ij}^2/\Delta E_{ij}^{(0)}$, where $\Delta E_{ij}^{(0)} = |E_i^{(0)} - E_j^{(0)}|$ is the AO energy difference between orbitals i and j , and H_{ij} is the resonance integral between the two AOs.
- The contribution to the anion band from the cation orbitals steadily increases from CaO to ScN to TiC. This is another effect of the changing electronegativities.

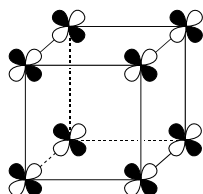
(56) ReO_3 adopts a perovskite-type structure, such as $SrTiO_3$, but with no atoms at the Sr atom positions. The structure is primitive cubic, space group $Pm\bar{3}m$, with Re atoms at the corners of the cubic unit cell and O atoms at the centers of every edge. Therefore, the structure is a 3-d network of vertex-sharing $[ReO_{6/2}]$ octahedra and the O atoms are linearly coordinated. The complex energy band structure and DOS curve can be understood using ligand field theory:

- The important valence AOs are O $2p$ and Re $5d$ functions, which separate into 3 t_{2g} orbitals below 2 e_g orbitals from the octahedral ligand field.
- Since O is a π -donor ligand, the t_{2g} orbitals are Re–O π -antibonding and the e_g orbitals are Re–O σ -antibonding.

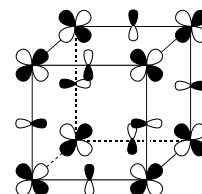
By counting valence electrons, ReO_3 has 25 valence electrons per formula unit with formally $d^1 \text{Re}^{6+}$ sites. Therefore, the O $2p$ bands are filled and there is 1 valence electron occupying the Re t_{2g} -band.

Energies in the band structure are plotted along various directions between the high symmetry points of the first Brillouin zone: Γ -X-M- Γ -R. For example, Γ -X and Γ -R, respectively, are parallel to the 4-fold and 3-fold axes of the structure. The t_{2g} -band is ~ 5 eV wide; its minimum is the triply degenerate Re–O nonbonding orbital at Γ and its maximum is a triply degenerate Re–O π -antibonding orbital at R:

Γ -point: No O $2p$ contributions due to requirements of translational symmetry, so this crystal orbital is Re–O nonbonding.



R-point: The phase changes from the Re $5d$ AOs allow overlap with O $2p$ AOs as Re–O π -antibonding.



In the DOS curve, the large peak around -3.0 eV corresponds to Re–O nonbonding states. The figure emphasizes the symmetry between Re–O π -bonding and π -antibonding states. The peak near -9.0 eV is from Re–O σ -bonding states. The Fermi level intersects the Re t_{2g} -band, and accounts for the metallic character of ReO_3 . Nearly isostructural WO_3 is semiconducting, while Na_xWO_3 and H_xWO_3 are metallic.

(57) The DOS is nicely verified from the valence band XPS spectrum although the relative intensities depend on the cross-sections for emission of photoelectrons from the different elements in the sample. For Mg $K\alpha$ incident radiation, states with significant Re contributions show higher intensities than those with more O contributions.

(58) *Populating Antibonding States – Distortions in Metal Trifluorides:*¹¹ In the cubic ReO_3 -type structure, the O atoms are linearly coordinated by two Re atoms. Down the $[111]$ direction of the cubic unit cell, there is a regular arrangement of octahedra, as seen in $d^2 \text{NbF}_3$, which may really be an oxyfluoride, $\text{NbO}_x\text{F}_{3-x}$. For $d^3 \text{MoF}_3$ and $d^5 \text{RuF}_3$, the cubic structure distorts to a rhombohedral structure by rotating the octahedra, which has two effects: (1) the bond angle at the F atoms is less than 180° , and (2) there are two orientations of the $[\text{MF}_{6/2}]$ octahedra, rotated to the left and to the right, because they are linked to each other like gears. If the rotation is carried to its ultimate extent, the $d^6 \text{RhF}_3$ structure with HCP fluoride ions is attained. Analysis of the M–F COHP diagram shows that the M–F π -antibonding interaction in the cubic structure becomes significant for valence electron counts exceeding d^2 . This destabilizing interaction is lowered by bending at the F atoms. In molecular examples, compare the change from linear CO_2 to bent O_3 .

The nature of the distortion of the cubic structure is that all nearest neighbor octahedra rotate in the opposite sense from the octahedron at the origin, i.e., the *phase* of the distortion alternates along the three unit cell axes. This distortion has translational symmetry appropriate for the R-point. In the band structure of cubic MF_3 , the top of the t_{2g} -band is at R; the bottom of the e_g -band is at Γ . Therefore, a *driving force* for this bending distortion is HOMO-LUMO mixing between the t_{2g} and e_g orbitals (bands) by a normal mode (phonon) that couples these two electronic states. The strength of this mixing varies inversely with the energy difference between the occupied and unoccupied electronic states.

¹¹ J. Lin, G.J. Miller, *Inorg. Chem.* **1993**, 32, 1476-1487.

(59) Populating Antibonding States – Vacancies in NbO:¹² NbO is a cubic structure with 3 formula units per unit cell that can be viewed as an ordered defect-NaCl arrangement with vacancies at Nb and O sites along the body diagonals of the cubic cells. A comparison of the DOS and COHP curves for a hypothetical NaCl-type structure and the actual structure of NbO have features that can help to explain the stability of the actual NbO structure:

- Only Nb–O bonding and nonbonding orbitals are filled; the Fermi level falls just below the presence of Nb–O antibonding states in the DOS. For the NaCl-type structure, Nb–O antibonding states would be occupied.
- Orbitals below the Fermi level are Nb–Nb bonding; at the Fermi level they are Nb–Nb nonbonding. For the NaCl-type model, Nb–Nb bonding states are not filled.

Therefore, in NbO, vacancies occur to optimize Nb–Nb bonding across the vacancies as well as to eliminate occupation of Nb–O antibonding states. Vacancies in molecules are more difficult to assess, but a series of molecular analogues exist in the *closo*-, *nido*-, and *arachno*-borane and carborane clusters.

(60) Populating Antibonding States – Ferromagnetism in 3d Metals: The 4d and 5d transition metals show regular variation in crystal structure as a function of valence electron count. In particular, from Group 5 to Group 11, the sequence is BCC-HCP-CCP. The 3d metals deviate from exact sequence, although Fe-Co-Ni follow the same structural sequence. As it turns out, these 3 metals are also ferromagnetic, which means that there is a magnetic moment associated with each atomic site and these moments line up to create net spontaneous magnetization for the solid. The *itinerant* ferromagnetism, arising from the conduction electrons, can be explained by relieving an electronic instability in the electronic structure of these metals.

Consider BCC iron as an example. The DOS curve using LDA, in which the two spin wavefunctions are degenerate, has 3 distinct peaks. Coupled with the COHP curve, the Fermi levels for metals with 5-6 valence electrons fall in a pseudogap with (nearly) optimized metal-metal interactions. However, Fe has 8 valence electrons, so its Fermi level falls on a large peak of the DOS that has significant Fe–Fe antibonding character. As seen in slides (56) and (57), some kind of structural distortion could occur. However, Fe chooses to break the degeneracy of spin-up and spin-down wavefunctions (by applying LSDA). As a result, the majority-spin band moves down in energy and the minority-spin band moves up in energy. Then, the total DOS has 4 distinct peaks, the Fermi level for Fe falls in a pseudogap, and orbital interactions within the spin-down COHP curve are nearly optimized. Integrating the DOS curves reveals that the net number of unpaired spins is 2.18, which agrees well with the saturated magnetization of $2.2 \mu_B$.

In an actual calculation, the LSDA approach is applied to an LDA result. If breaking the spin degeneracy is favored, then the calculation will achieve a new converged result. If breaking the spin degeneracy is not favored, then the calculation will converge to the same outcome as with LDA. Breaking the spin degeneracy for these 3d metals is caused in part because there are no *d*-type core orbitals, so the 3d AOs feel a significant effective nuclear charge. Molecular analogues include the preference of π -bonding for the second-period elements C, N, and O, for which their valence *p* AOs have no core *p* orbitals.

¹² J.K. Burdett, T. Hughbanks, *J. Am. Chem. Soc.* **1984**, *106*, 3101-xxxx.

(61) An excellent *pocket-sized* book that is written particularly for chemists is *Solids and Surfaces: A Chemist's View of Bonding in Extended Structures* by Roald Hoffmann, published in 1988. This booklet summarizes the results presented in three review articles published by Prof. Hoffmann and his group. Another reference is a larger review article "Chemical Bonding in Solids" by G.J. Miller, Y. Zhang, and F. Wagner, published in *Handbook of Solid State Chemistry*.

Some General References:

1. D. Pettifor, *Bonding and Structure of Molecules and Solids*; Clarendon Press: Oxford, 1995.
2. W.A. Harrison, *Elementary Electronic Structure, Revised Ed.* World Scientific: New Jersey, 2004.
3. R. Dronskowski, *Computational Chemistry of Solid State Materials*; Wiley-VCH: Weinheim, Germany, 2005.
4. E. Canadell, M.-L. Doublet, C. Iung, *Orbital Approach to the Electronic Structure of Solids*, Oxford University Press: New York, 2012.